Antibunched two-mode two-photon bundles via atomic coherence

Chengdeng Gou,[1] Xiangming Hu,[1,*] and Fei Wang[2]
[1]*College of Physical Science and Technology, Central China Normal University, Wuhan 430079, People's Republic of China*
[2]*School of Science, Hubei University of Technology, Wuhan 430068, People's Republic of China*

(Received 25 July 2022; accepted 12 December 2022; published 23 December 2022)

In this paper we propose an efficient scheme to continuously generate two-mode two-photon bundles by using a three-level atomic system, in which two correlated channels are created for the bundle emission in different modes. It is shown that the antibunching effect not only happens between the same modes but also between two different modes. While the former is due to the dominance of cavity decay over atomic decay, the latter is based on the atomic coherence between the two final states of bundle emission. The antibunched two-mode two-photon bundles are achievable in a wide range of parameters and robust against environmental noise. This scheme provides a kind of photon sources for two-signal-based applications such as quantum information processing, high-precision metrology, and ultrasensitive biosensing.

DOI: 10.1103/PhysRevA.106.063718

I. INTRODUCTION

Nonclassical states of light are a major premise for the implementation of photonic quantum technologies [1]. The single-photon sources, which are closely related to antibunching behavior and sub-Poissonian distribution, are viewed as a fundamental topic in quantum optics all the time because they can find potential applications in quantum computation [2–4] and quantum information processing [5,6]. More interestingly, the N-photon sources, emitting more than one photon, are also the heart of many recent quantum technological applications including high-NOON states [7], quantum communication [8], quantum metrology [9], lithography [10], spectroscopy [11,12], and biological sensing [13,14]. Recently, a novel scheme as a promising candidate to generate N-photon resources has been proposed. That is, an emitter releases the optical energy strictly by strongly correlated N-photon quanta, which behaves like a single physical entity called the N-photon bundle. This has attracted much attention and has been extended to various quantum systems such as cavity quantum electrodynamics (QED) systems [15–21], circuit QED systems [22,23], trapped atom systems [24], macroscopic mechanical resonators [25], and so on.

For the cavity QED setup containing a two-level atom [15], it is explored that by pumping the atom into a highly excited state, the continuous emission of the multiple photons is crucially based on the Purcell effect enhanced internal leapfrog processes, in which a super-Rabi oscillation is established between the ground state and the higher-excited N-photon Fock state. Successively, the conditions are relaxed into bad-cavity situations, where one can reveal and purify multiphoton emission just by frequency filtering [18]. Interestingly, in an acoustic cavity QED system, Bin *et al.* have proposed an efficient method for producing high-purity N-phonon bundle emission based on the Stokes process [19]. A parity-symmetry-protected scheme is proposed to generate a perfect $2N$-photon bundle emission in the ultrastrong-coupling regime [20]. Furthermore, the multiphoton bundle emission has also been investigated in a Josephson-photonics circuit [22] and in the N-photon Jaynes-Cummings model [26], respectively. However, so far the existing schemes have been confined mainly to the two-level quantum emitters and so to a single mode.

Here we present a scheme for generating the antibunched two-photon bundles in two different cavity modes. Bundle antibunching appears not only between the same modes but also between the different modes. The two-photon bundles are obtained from the leapfrog transitions, respectively, at the different inner sidebands of the dressed three-level atom. Different from the previous schemes, two channels for bundle emission in different modes coexist in our scheme and atomic coherence plays a crucial role. The two needed channels for the bundle emission are preserved selectively, and at the same time the bundles in the different modes are antibunched. It is also shown that the bundle emission and the antibunching are obtainable in a wide range of parameters and are robust against thermal noise. The two-mode two-photon bundles as heralded single-photon sources can be used in quantum information processing, such as quantum key distribution [6,27,28], quantum teleportation [29,30], entanglement swapping [31,32], and quantum repeaters [33], where two different signals in nonclassical states are required. Such nonclassical sources of light are also applicable in high-precision quantum metrology [34] and ultrasensitive biosensing [35].

The remainder of the paper is organized as follows: In Sec. II, we present a general introduction to the model. In Sec. III, we derive the conditions of multiphoton resonance transition in the dressed picture and explore the multiphoton leapfrog processes through the correlation function. In Sec. IV, the dynamical emission properties of two-mode two-photon bundles are discussed in detail. In Sec. V, we discuss

*xmhu@ccnu.edu.cn.

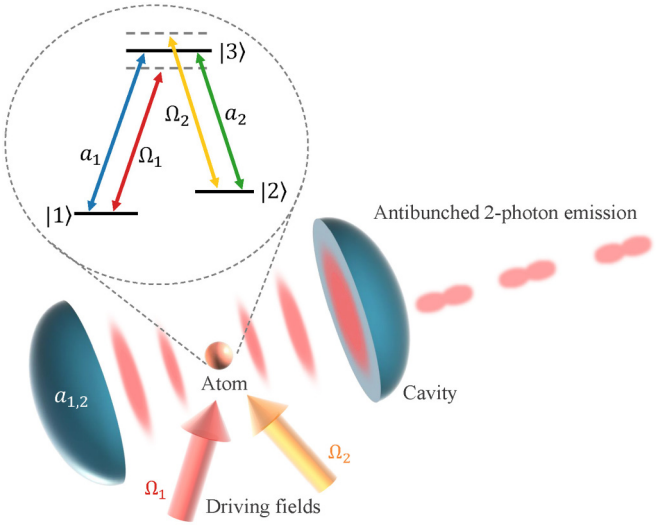

FIG. 1. Sketch of a three-level Λ-configuration atom strongly coupled to two cavity modes, a_1 and a_2. Two coherent fields, Ω_1 and Ω_2, drive the $|1\rangle \leftrightarrow |3\rangle$ and $|2\rangle \leftrightarrow |3\rangle$ transitions, respectively. At a proper driving frequency, the system emits consecutive two-photon bundles.

the effect of nonsymmetric parameters on two-mode two-photon bundles. A conclusion is given in Sec. VI.

II. MODEL AND EQUATIONS

As shown in Fig. 1, a three-level atom consisting of two ground states, $|1\rangle$ and $|2\rangle$, and an excited state, $|3\rangle$, is placed in a two-mode cavity. Two monochromatic lasers of frequencies ω_1 and ω_2 are applied to two atomic transitions, $|1\rangle \leftrightarrow |3\rangle$ and $|2\rangle \leftrightarrow |3\rangle$, with Rabi frequencies Ω_1 and Ω_2, respectively. At the same time, two cavity modes of frequency, ω_{a_1} and ω_{a_2}, are strongly coupled to the transitions $|1\rangle \leftrightarrow |3\rangle$ and $|2\rangle \leftrightarrow |3\rangle$ with coupling strengths g_1 and g_2, respectively.

In the electric dipole and rotating-wave approximations, the Hamiltonian of this bimodal cavity-QED system consists of two parts, $H = H_a + H_c$, with (hereafter $\hbar = 1$)

$$\begin{aligned} H_a =& \Delta_1\sigma_{33} + (\Delta_1 - \Delta_2)\sigma_{22} + \Omega_1(\sigma_{31} + \sigma_{13}) \\ &+ \Omega_2(\sigma_{32} + \sigma_{23}), \end{aligned} \tag{1}$$

$$\begin{aligned} H_c =& \delta_1 a_1^\dagger a_1 + \delta_2 a_2^\dagger a_2 + g_1(a_1\sigma_{31} + a_1^\dagger\sigma_{13}) \\ &+ g_2(a_2\sigma_{32} + a_2^\dagger\sigma_{23}). \end{aligned} \tag{2}$$

The first term represents the interaction of the atom with classical driving fields and the second term describes the two cavity modes that interact with the two atomic transitions, respectively. Here $\sigma_{ij} = |i\rangle\langle j|$ ($i, j = 1$, 2, and 3) are the projection operators for $i = j$ and the spin-flip operators for $i \neq j$. a_l and $a_l^\dagger$ are the annihilation and creation operators for two cavity modes. $\Delta_l = \omega_{3l} - \omega_l$ ($l = 1$ and 2) are the detunings of atomic transition frequencies ω_{3l} with respect to driving field frequencies ω_l. $\delta_l = \omega_{a_l} - \omega_l$ ($l = 1$ and 2) are the detunings of cavity frequencies ω_{a_l} with respect to driving field frequencies ω_l.

The dynamical evolution of the system is governed by the master equation [36,37]

$$\dot{\rho} = -i[H, \rho] + \sum_{l=1,2}\left(\frac{\kappa_l}{2}\mathcal{L}[a_l]\rho + \frac{\gamma_l}{2}\mathcal{L}[\sigma_{l3}]\rho\right), \tag{3}$$

where $\mathcal{L}[a_l]\rho$ and $\mathcal{L}[\sigma_{l3}]\rho$ are the Lindblad terms describing the cavity and atomic decays with rates κ_l and γ_l, respectively, and they take the form $\mathcal{L}[o]\rho = 2o\rho o^\dagger - o^\dagger o\rho - \rho o^\dagger o$. This master equation can be solved numerically by using the PYTHON package QUTIP [38], which provides a convenient and effective way to study the dynamics of photon emission in the system.

In order to clarify the mechanism of the multiphoton resonance, it is necessary for us to turn to the dressed-state picture for analytical analysis. For arbitrary atom-driving-field detunings and Rabi frequencies, the dressed atom nonlinearities are generally so complicated that they conceal the interaction mechanisms for the quantum correlations. Therefore, it is better for us to choose the symmetric case for the atom-field detunings $\Delta_1 = -\Delta_2 = \Delta$ and equal Rabi frequencies $\Omega_1 = \Omega_2 = \Omega$. Under the strong driving conditions $\Omega \gg (g_{1,2}, \kappa_{1,2}, \gamma_{1,2})$, the dressed states are obtained through diagonalizing the Hamiltonian H_a and expressed in terms of the bare states as [39]

$$\begin{aligned} |+\rangle =& \frac{1-s}{2}|1\rangle + \frac{1+s}{2}|2\rangle + \frac{c}{\sqrt{2}}|3\rangle, \\ |0\rangle =& \frac{c}{\sqrt{2}}|1\rangle - \frac{c}{\sqrt{2}}|2\rangle + s|3\rangle, \\ |-\rangle =& \frac{1+s}{2}|1\rangle + \frac{1-s}{2}|2\rangle - \frac{c}{\sqrt{2}}|3\rangle, \end{aligned} \tag{4}$$

where we define $c = \sqrt{2}\Omega/\bar{\Omega}$, $s = \Delta/\bar{\Omega}$, and $\bar{\Omega} = \sqrt{\Delta^2 + 2\Omega^2}$. The dressed states $|0\rangle$ and $|\pm\rangle$ correspond to equally spaced eigenenergies $E_0 = \Delta$ and $E_\pm = \Delta \pm \bar{\Omega}$. The Hamiltonian H_a takes the free form $H_a = \bar{\Omega}(\sigma_{++} - \sigma_{--})$, where we have removed the common term Δ of all eigenenergies; i.e., we have set E_0 to the energy reference point. σ_{ij} ($i, j = +$, 0, and $-$) have been defined as the projection operators ($i = j$) and spin-flip operators ($i \neq j$). Spontaneous transitions from an upper triplet of dressed states to the lower adjacent triplet lead to a five-peaked structure of fluorescence spectrum [36]. According to the frequency components of the fluorescence spectrum, the bare atomic operators can be divided into several terms as

$$\sigma_{l3} = \sigma_{2L}^{(l)} + \sigma_L^{(l)} + \sigma_0^{(l)} + \sigma_R^{(l)} + \sigma_{2R}^{(l)}, \tag{5}$$

where $\sigma_0^{(l)}$, $\sigma_{L,R}^{(l)}$, and $\sigma_{2L,2R}^{(l)}$ denote the dressed atomic transitions at the central frequency ω_l, the inner sidebands $\omega_l \pm \bar{\Omega}$, and the outer sidebands $\omega_l \pm 2\bar{\Omega}$, respectively. They are defined as $\sigma_L^{(1)} = A_+\sigma_{-0} + B\sigma_{0+}$, $\sigma_R^{(1)} = A_-\sigma_{+0} - B\sigma_{0-}$, $\sigma_{2L}^{(1)} = C_+\sigma_{-+}$, $\sigma_{2R}^{(1)} = -C_-\sigma_{+-}$, and $\sigma_0^{(1)} = C_-\sigma_{++} - C_+\sigma_{--} + D\sigma_{00}$ and as $\sigma_L^{(2)} = A_-\sigma_{-0} - B\sigma_{0+}$, $\sigma_R^{(2)} = A_+\sigma_{+0} + B\sigma_{0-}$, $\sigma_{2L}^{(2)} = C_-\sigma_{-+}$, $\sigma_{2R}^{(2)} = -C_+\sigma_{+-}$, and $\sigma_0^{(2)} = C_+\sigma_{++} - C_-\sigma_{--} - D\sigma_{00}$, with the coefficients $A_\pm = s(1 \pm s)/2$, $B = c^2/2$, $C_\pm = c(1 \pm s)/2\sqrt{2}$, and $D = cs/\sqrt{2}$. With these representations, we can clearly understand the spontaneous emission processes of the dressed

atom and its interaction with the cavity fields. By adjusting cavity frequency to resonate or not with the atomic transition, the corresponding emission can be effectively increased or decreased. In this way, under the strong-excitation regime, multiphoton sideband emission can be obtained in the cavity quantum electrodynamics.

III. MULTIPHOTON RESONANT TRANSITION

Multiphoton emission related to nonlinear dynamics can be analyzed more clearly in a dressed picture in which the interaction of the driving fields is merged into the atom. Choosing the symmetric detunings of the cavity fields from the driving fields $\delta_1 = -\delta_2 = \delta$, we analytically derive the frequency condition for multiphoton sideband resonance transitions and numerically simulate the photon correlation functions. For the sake of simplicity, we assume the same coupling strengths $g_1 = g_2 = g$ and decay rates $\kappa_1 = \kappa_2 = \kappa$ and $\gamma_1 = \gamma_2 = \gamma$.

In a strong-driving regime, the atom-field interaction provides high-order nonlinearities for multiphoton transitions, which are generally hidden behind the single-photon processes. However, they can be enhanced by the Purcell effect via cavity modes. Similar to the "N-photon leapfrog" processes in the Mollow triplet [40,41], we introduce the counterparts in the three-level system, where the photon emission processes are richer than that of two-level systems. The N-photon leapfrog processes occur when the sum of N-photon energies in each cavity mode matches the allowed transitions between dressed states, i.e., $N\delta = \Delta_E$, with $\Delta_E = \pm\bar{\Omega}$ and $\pm 2\bar{\Omega}$.

Specifically, we focus on the resonance conditions, where the two cavity modes are resonant respectively with the two atomic dipole-allowed transitions, i.e., $\omega_{a_l} = \omega_{3l}$ (i.e., $\delta = \Delta \neq 0$). It should be noted that photon emission will not happen at $\delta = 0$ owing to the effect of coherent population trapping. At the same time, since the energies of a single photon in the two modes failed to match the transitions between dressed states, the single-photon processes are suppressed and thus the multiphoton transitions become dominant. The multiphoton resonance transitions and the corresponding conditions can be summarized as

$$\left.\begin{aligned} |\pm\rangle &\xrightarrow{N} |0\rangle \\ |0\rangle &\xrightarrow{N} |\mp\rangle \end{aligned}\right\}, \quad \Delta_N^{\pm} = \pm\sqrt{\frac{2\Omega^2}{N^2-1}} \quad (N>1), \tag{6}$$

$$|\pm\rangle \xrightarrow{N} |\mp\rangle, \quad \tilde{\Delta}_N^{\pm} = \pm\sqrt{\frac{8\Omega^2}{N^2-4}} \quad (N>2), \tag{7}$$

where $|i\rangle \xrightarrow{N} |j\rangle$ denotes that the dressed-atom transition from state $|i\rangle$ to state $|j\rangle$ and the two modes obtain N photons simultaneously. These processes correspond respectively to the multiphoton emission at the inner sidebands as in Eq. (6) and at the outer sidebands as in Eq. (7). Since the two cavity modes respectively couple to the different atomic transitions, this mechanism gives us an opportunity to generate photon bundles of two different frequencies.

In order to describe the multiphoton emission mechanism as above, we use Eq. (3) and calculate the nth-order quantum correlation functions [42]

$$g_{(ll)}^{(n)}(0) = \frac{\langle a_l^{\dagger n} a_l^n\rangle}{\langle a_l^{\dagger} a_l\rangle^n} = \frac{\mathrm{tr}\left(\rho_{\mathrm{ss}} a_l^{\dagger n} a_l^n\right)}{[\mathrm{tr}(\rho_{\mathrm{ss}} a_l^{\dagger} a_l)]^n}, \tag{8}$$

for the cavity mode a_l at steady state ($\dot{\rho} = 0$). In Fig. 2(a), we plot the equal-time nth-order correlation functions $g_{(ll)}^{(n)}(0)$ ($n = 2$ and 3) as functions of δ/g. In Fig. 2(b), we also plot the photon-number distributions $P_m^{(l)} = \mathrm{tr}(|m\rangle\langle m|_l \rho_{\mathrm{ss}})$, where $m = 0$–4 is the photon number in the mode a_l. In the symmetric case, the properties of photon emission in two cavity modes are identical, i.e., $g_{(11)}^{(n)}(0) = g_{(22)}^{(n)}(0)$ and $P_m^{(1)} = P_m^{(2)}$. It is seen from Fig. 2(a) that the bunching exists over all ranges of detunings since we always have $g_{(ll)}^{(n)}(0) > 1$. The bunching peaks or dips in correlation functions $g_{(ll)}^{(n)}(0)$ correspond to the multiphoton transitions. N-photon transitions at sidebands, which are denoted by $S^{(N)}$, are strongly related to the photon-number distributions $P_m^{(l)}$ in Fig. 2(b). At $\delta = \pm 24.5g$, since $P_1^{(l)}$ and $P_2^{(l)}$ have the same order of magnitude, this means the occurrence of the two-photon leapfrog transitions $S^{(2)}$. Similarly, the peaks located at $\delta = \pm 15g$ correspond to the three-photon leapfrog transitions $S^{(3)}$ since $P_3^{(l)}$ has the same order of magnitude value as $P_2^{(l)}$. Namely, the same intensities of $P_{N-1}^{(l)}$ and $P_N^{(l)}$ indicate N-photon resonance transitions at $\delta = \Delta_N^{\pm}$. It is found that the numerical calculations are in good agreement with our analysis. In particular, the two dips instead of peaks at the two-photon resonance $\delta = \pm 24.5g$ indicate

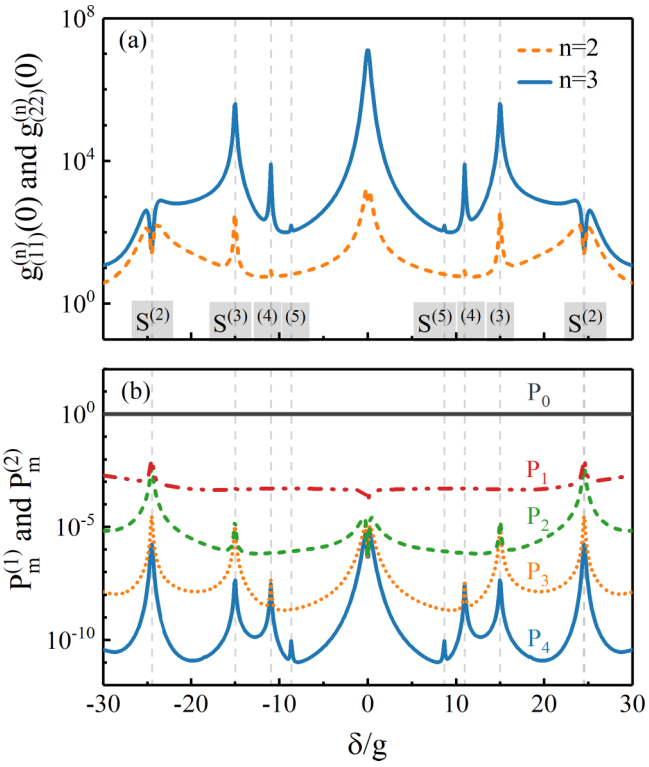

FIG. 2. (a) Equal-time nth-order correlation functions $g_{(11)}^{(n)}$ and $g_{(22)}^{(n)}$ for $n = 2$ and 3, and (b) photon-number distributions $P_m^{(1)}$ and $P_m^{(2)}$ for $m = 0$–4 as functions of δ/g. Here the parameters are $\Delta = \delta$, $\kappa/g = 0.1$, $\gamma/g = 0.01$, and $\Omega/g = 30$. The gray dashed vertical lines label the locations of N-photon resonances $S^{(N)}$ at sidebands.

that the system enters a regime of pure two-photon bundle emission.

IV. TWO-PHOTON BUNDLE EMISSION

Multiphoton bundle emission differs from traditional photon emission in that the photons in a bundle are emitted simultaneously, which means they behave like a single physical entity and have a much stronger correlation. Although such a phenomenon is predicted by the bunching dips of $g^{(n)}_{(ll)}(0)$, the mechanism for it does not clear. Therefore, new methods have been explored to characterize the properties of photon bundle emission [15] for the further development of the source of the quantum light. In this section, we discuss the two-photon bundle emission at $\delta = \Delta = 24.5g$ in detail.

To identify such novel photon emission, a correlation function describing the statistics of photon bundles is introduced [15]:

$$g^{(n)}_N(t_1,\ldots,t_n) = \frac{\langle \mathcal{T}_-\{\prod_{i=1}^n a^{\dagger N}(t_i)\}\mathcal{T}_+\{\prod_{i=1}^n a^N(t_i)\}\rangle}{\prod_{i=1}^n \langle a^{\dagger N}a^N\rangle(t_i)}, \quad (9)$$

where $\mathcal{T}_\pm$ represent the time ordering operators. Compared to the traditional n-order correlation function, this function uses a bundle of N photons instead of each individual photon as a unit. If $N = 1$, the new correlation function reduces to the transitional nth-order correlation function. For $N = 2$, this time-delayed second-order correlation function is written in the form

$$g^{(2)}_{2(lk)}(\tau) = \frac{\langle a_l^{\dagger 2}(0)a_k^{\dagger 2}(\tau)a_k^2(\tau)a_l^2(0)\rangle}{\langle (a_l^{\dagger 2}a_l^2)(0)\rangle\langle (a_k^{\dagger 2}a_k^2)(\tau)\rangle}, \quad (10)$$

which is extended to describe the correlations between two common or different modes ($l, k = 1$ and 2). For $l = k$, $g^{(2)}_{2(lk)}(\tau)$ represents the autocorrelation function of two-photon bundles in the same mode, where $\tau \geqslant \tau_{\min} = \sum_{m=1}^N 1/m\kappa$. $\tau_{\min}$ can be approximately regarded as zero-time delay since the small-time windows of width $1/\kappa$ center at zero, and the bundle correlation function $g^{(2)}_{2(ll)}(\tau)$ is ill-defined (as such short times probe inside the bundle itself) [15,20]. While for $l \neq k$, $g^{(2)}_{2(lk)}(\tau)$ ($\tau \geqslant 0$) represents the cross-correlation function between the two-photon bundles in different modes. Such correlations can be measured directly thanks to the developments in two-photon detection [43]. In Fig. Fig. 3, we plot the time-delayed second-order autocorrelation functions $g^{(2)}_{(ll)}(\tau)$ and $g^{(2)}_{2(ll)}(\tau)$ ($l = 1$ and 2) and the cross-correlation function $g^{(2)}_{2(12)}(\tau)$ at $\delta = \Delta = 24.5g$. It can be seen that $g^{(2)}_{(11)}(0) = g^{(2)}_{(22)}(0) > 1$ and $g^{(2)}_{2(11)}(\tau_{\min}) = g^{(2)}_{2(22)}(\tau_{\min}) < 1$ at zero time, which guarantees the generation of antibunched two-photon bundles in the same mode. At the same time, the two-photon bundles between different modes are also antibunching, i.e., $g^{(2)}_{2(12)}(0) < 1$. When the timescale is small, the antibunching between the bundles in different modes a_1 and a_2 is stronger than that of bundles in the same mode a_1 (a_2). However, when the timescale is large enough, the correlation between bundles in different modes a_1 and a_2 has the same strength as the correlation between the bundles in the same mode a_1 (a_2). This manifests the alternate appearance of the two-photon bundles in the two modes.

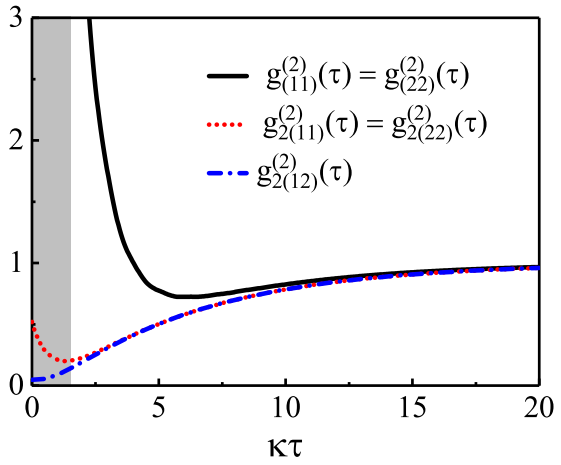

FIG. 3. Time-delayed autocorrelation functions $g^{(2)}_{(ll)}$ and $g^{(2)}_{2(ll)}$ ($l = 1$and 2) and the cross-correlation function $g^{(2)}_{2(12)}$. We consider $\delta = \Delta = 24.5g$ and the other parameters are the same as those in Fig. 2.

In order to clarify such bundle emissions, it is necessary to analyze their transition paths. According to the resonance conditions in Eqs. (6) and (7), we notice that there are two categories of transition path for the two cavity modes when the system undergoes two-photon processes. One of them is related to inner sideband transitions and the other is related to outer sideband transitions as $\tilde{\Delta}_4^{\pm} = \Delta_2^{\pm}$. The transitions at the outer sidebands in Eq. (7) can be safely discarded because they involve a cascade transition (composed of two second-order processes and passing through a real state) that causes the correlation of similar strength with a third-order process [40]. The rest of the transitions in Eq. (6) are mainly affected by two aspects. As shown in Fig. 4(a), population inversion $\langle\sigma_{00}\rangle_{\rm ss} > \langle\sigma_{\pm\pm}\rangle_{\rm ss}$ happens in the entire region of the multiphoton resonance $|\Delta| < \Omega$. At the same time, according to the effective Hamiltonian, Eqs. (A5)–(A13), derived in the Appendix, the absolute value of coefficients $|G_{1,2,3}|$ and $|\tilde{G}_{1,2,3}|$ as functions of detuning Δ/g are plotted in Fig. 4(b) at two-photon resonances $\delta = \pm\bar{\Omega}/2$. One can see that the coefficients $|G_1|$ and $|\tilde{G}_1|$ (solid lines) increase rapidly with the increasing of $|\Delta|/g$, while $|G_2|$ and $|\tilde{G}_2|$ (dashed lines) first decrease and then increase, leading to the inter-

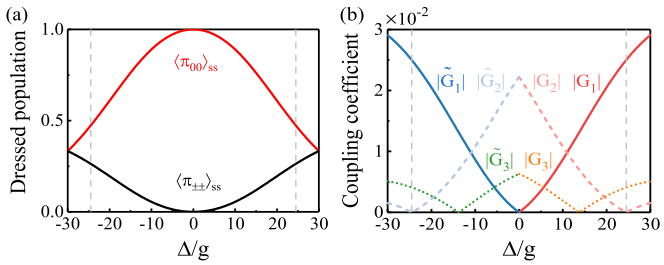

FIG. 4. (a) The steady-state dressed population $\langle\sigma_{00}\rangle_{\rm ss}$ and $\langle\pi_{\pm\pm}\rangle_{\rm ss}$ as functions of the detuning Δ/g. (b) The coefficients $|G_{1,2,3}|$ and $|\tilde{G}_{1,2,3}|$ in the effective Hamiltonian derived in the Appendix. The two-photon resonance condition is chosen as $\delta = \pm\bar{\Omega}/2$ and the other parameters are the same as those in Fig. 2. The gray dashed lines label the special points at $\Delta/g \approx \pm 24.5$.

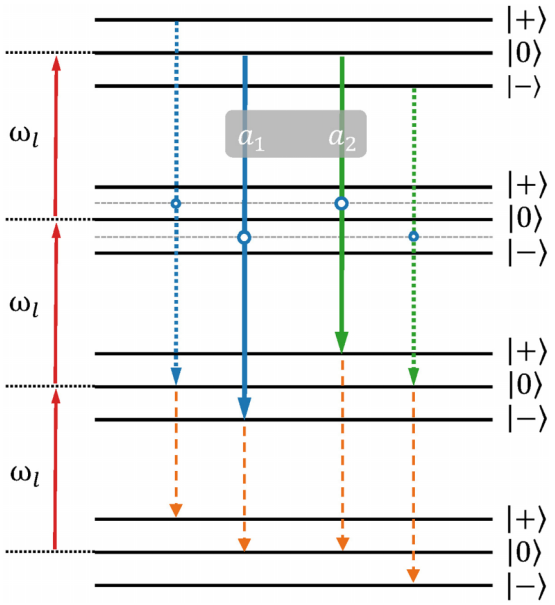

FIG. 5. The dressed-state structure under the condition of the two-photon resonance $\delta = \Delta = \Delta_2^+$. The solid blue and green lines correspond to the preserved two-photon bundle emission and the dotted blue and green lines correspond to the eliminated emission. The yellow dashed lines depict the subsequent emission which brings the system back to the initial states.

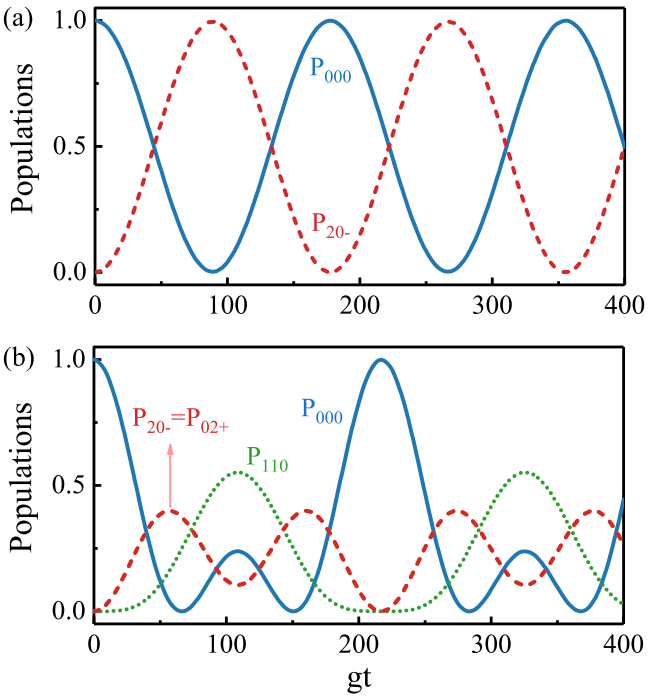

FIG. 6. (a) Time evolutions of the population of the states P_{000} and P_{20-} when $g_1 = g$ and $g_2 = 0$. (b) Time evolutions of the population of the states P_{000}, P_{20-}, P_{02+}, and P_{110} when $g_1 = g_2 = g$. We consider the condition of the initial state $|0, 0, 0\rangle$ and the two-photon resonance $\delta = \Delta = 24.5g$. The driving strength is chosen as $\Omega = 30g$.

sects at $|\Delta|/g = 10.95$. When $|\Delta|/g > 10.95$, i.e., $|G_1| > |G_2|$ ($|\tilde{G}_1| > |\tilde{G}_2|$), it means that the coupling terms $\sigma_{0-}a_1^2$ and $\sigma_{0+}a_2^2$ ($\sigma_{0+}a_1^2$ and $\sigma_{0-}a_2^2$) have more weight than that of $\sigma_{+0}a_1^2$ and $\sigma_{-0}a_2^2$ ($\sigma_{-0}a_1^2$ and $\sigma_{+0}a_2^2$), and vice versa. It is the atomic coherence induced by the strongly driven fields and quantum interference that work together to affect dressed populations and cross couplings. Two cavity modes respectively couple to different transitions, which guarantees the generation of two-photon bundles at two different frequencies.

Moreover, in Fig. 4(b), it should be pointed out that the coefficients $|G_2|$ and $|\tilde{G}_2|$ are vanishing at $\Delta \approx \pm 24.5g$; thus, the influence of corresponding transition paths, i.e., $|\pm\rangle \rightleftarrows |0\rangle$, will be completely eliminated via destructive interference. In other words, if $\delta = \Delta = \Delta_2^{\pm}$, the system experiences two two-photon transitions $|0\rangle \rightleftarrows |\mp\rangle$ selectively. As is shown in Fig. 5, the blue and green solid lines respectively represent the preserved two-photon bundle transitions in the a_1 and a_2 modes, while the blue and green dashed lines represent the eliminated transitions. Although the coefficients $|G_3|$ and $|\tilde{G}_3|$ are nonzero, the corresponding simultaneous emission of the a_1 photon and the a_2 photon can be ignored since it is related to the transition between the states $|\pm\rangle \rightleftarrows |\pm\rangle$ without atomic population inversion. Such simplified transitions ensure more perfect emission of the two-photon bundle. Including the two-photon emission (the solid green and blue lines) and the subsequent radiation to the initial state $|0\rangle$ (the dashed yellow lines) in the dressed picture, the energy of the whole photon-emission process is conserved under three quantum excitations (the solid red lines). If cavity decay dominates over atomic decay, the two-photon bundles in the same modes will be blockaded by the spontaneous emission of the atom, resulting in an antibunching property. Moreover, the antibunching exists between the two-photon bundles in the different modes since the final states of the two-photon transition of the two modes are coherent.

Two-photon bundle transitions can be manifested by super-Rabi oscillation. At $\delta = \Delta = 24.5g$, according to Eqs. (A5) and (A6) derived in the Appendix, the effective Hamiltonian can be rewritten as

$$\begin{aligned} H_{\rm eff}^{(2)} =& g_{{\rm eff},1}^{(2)} a_1^2 \sigma_{0-} + g_{{\rm eff},2}^{(2)} a_2^2 \sigma_{0+} + {\rm H.c.} \\ =& \sum_{\mu,\nu=0}^{\infty} \Big[g_{{\rm eff},1}^{(2)} \sqrt{(\mu+1)(\mu+2)} |\mu, \nu, 0\rangle\langle \mu+2, \nu, -| \\ & + g_{{\rm eff},2}^{(2)} \sqrt{(\nu+1)(\nu+2)} |\mu, \nu, 0\rangle\langle \mu, \nu+2, +| \Big] + {\rm H.c.}, \end{aligned} \tag{11}$$

where we have ignored the eliminated terms $a_1^2\sigma_{+0}$ and $a_2^2\sigma_{-0}$ and have defined

$$g_{{\rm eff},l}^{(2)} = -\frac{2g_l^2}{3\bar{\Omega}} [3A_+(C_+ + D) + A_- C_+]. \tag{12}$$

Here, states $|m_1, m_2, i\rangle = |m_1\rangle \otimes |m_2\rangle \otimes |i\rangle$ represent that cavity mode a_1 possesses m_1 photons, mode a_2 possesses m_2 photons, and the atom is located in the dressed state $|i\rangle$. It can be seen from Eq. (11) that two different states are coupled to a common state in square brackets. This means that there are two transition paths for generating two-mode two-photon bundles. To observe such oscillations, we plot in Fig. 6 the nonzero populations $P_{m_1 m_2 i} = |\langle m_1, m_2, i|\psi(t)\rangle|^2$ without dissipation. The initial state of the system is assumed

to be $|0,0,0\rangle$; i.e., the two cavity modes are both prepared in a vacuum state and the atom is located in the dressed state $|0\rangle$. At first, we consider the case that there is only one mode that exists, e.g., $g_1 = g$, $g_2 = 0$. The time evolutions of nonzero populations P_{000} and P_{20-} are plotted in Fig. 6(a). It can be seen that the whole system will oscillate back and forth between state $|0,0,0\rangle$ and state $|2,0,-\rangle$. Namely, the two-photon bundle in mode a_1 can be solely generated and is accompanied by a dressed-atom flip $|0\rangle \to |-\rangle$. When both two cavity modes are considered, i.e., $g_1 = g_2 = g$, the situation becomes different. In Fig. 6(b) we present all the states that have a nonzero population. It is found that the two populations P_{20-} and P_{02+} have the same behavior of oscillation. A peak in the single-mode case splits into two peaks when both of the two modes are contained. This means that the emission of two-photon bundles in two modes is separately accompanied by different atomic flips. Besides, we find that these two transition paths are coherent since the oscillations of the off-diagonal elements of states $|2,0,-\rangle$ and $|0,2,+\rangle$ are consistent with the oscillations of their diagonal elements. It is established by the intrinsic atomic coherence between the dressed states. It is for this reason that the two-photon bundles between the different modes have strong antibunching properties. During the two-photon transitions for two channels, the intermediate state $|1,1,0\rangle$ appears, which means that there is a possibility to generate photon pairs composed of one a_1 photon and one a_2 photon. However, this is a negligible process since it is just the oscillation between P_{110} and P_{000} without population inversion for light amplification.

To display two-photon bundle emission more intuitively, we simulate the actual situation of photon radiation by extracting the photon emission event from Monte Carlo simulation over 25 quantum trajectories. We separately simulate two cases for the existence of a single cavity mode and double cavity modes. Shown in Fig. 7, the horizontal and vertical axes respectively represent time and trajectory, and each point indicates a photon emission event. In Fig. 7(a), when only one mode exists, it can be seen that the two-photon events account for the majority of the whole radiation processes in addition to a small fraction of unexpected events. In Fig. 7(b), the two-photon events still possess a large proportion when two modes are contained. It shows that the two-photon bundle emissions in the two different modes are random in times and trajectories. Although a small part of two-photon events composed of one a_1 photon and one a_2 photon are generated, it is negligible compared to the two-photon bundle generated separately by the two modes. Therefore, two-mode two-photon bundles are achievable in our scheme.

Next, we focus on how the correlation of two-photon bundle emission varies with atomic decay. Since the two cavity modes have the same properties, we only present the function of mode a_1. In Fig. 8(a), the time-delayed bundle correlation function $g^{(2)}_{2(11)}(\tau)$ as a function of γ/g is plotted. It shows how the statistics of the photon bundle changes from bunching to antibunching as atomic decay decreases, passing through the coherent emission with $g^{(2)}_{2(11)}(\tau) = 1$. This can be interpreted by the fact that the long-lived atom (sufficiently small γ) ensures that the timescale of radiation between photon bundles is much larger than that of photon radiation within bundles. As a result, the two adjacent bundles exhibit antibunching

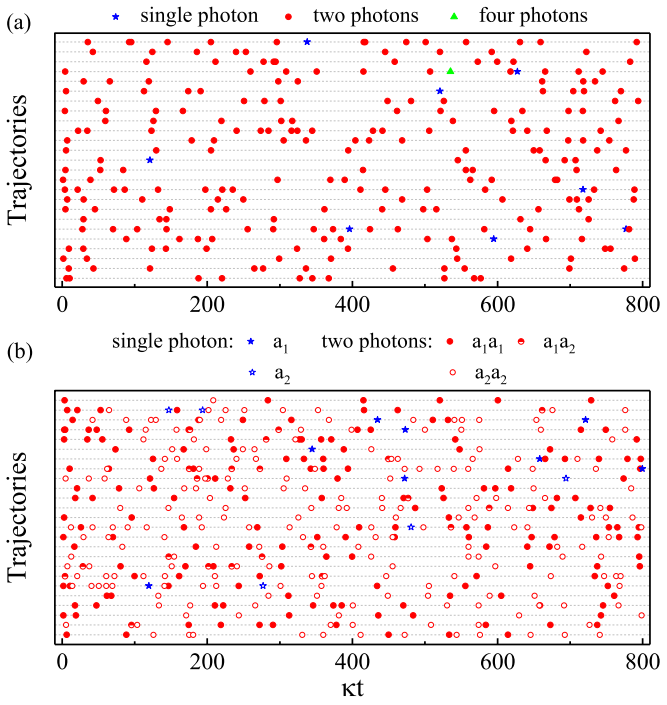

FIG. 7. A series of emission events extracted from the Monte Carlo simulations over 25 quantum trajectories for two-photon resonance for (a) the single mode case, $g_1 = g$ and $g_2 = 0$, and (b) the two-mode case, $g_1 = g_2 = g$. The single-, two-, and four-photon emissions in mode a_1 (a_2) are denoted by solid (hollow) blue stars, red circles, and green triangles, respectively. The other parameters are the same as those in Fig. 3.

properties. This feature can be seen clearly in Fig. 8(b). The shadow area satisfies the conditions $g^{(2)}_{2(11)}(\tau_{\min}) < 1$, $g^{(2)}_{2(12)}(0) < 1$, and $g^{(2)}_{(11)}(0) > 1$, which describe the antibunched two-mode two-photon bundles. It should be pointed out that the cross-correlation function of the two-photon bundle $g^{(2)}_{2(12)}(0)$ is always less than or equal to 1 due to the relatively stable atomic coherence of our system.

Finally, we explore the influence of thermal photon noise on the antibunched two-photon bundles. To do this, we include the dissipative terms $\sum_{l=1,2} \frac{n_{\mathrm{th},l}\kappa_l}{2}(\mathcal{L}[a_l]\rho + \mathcal{L}[a_l^\dagger]\rho)$ in

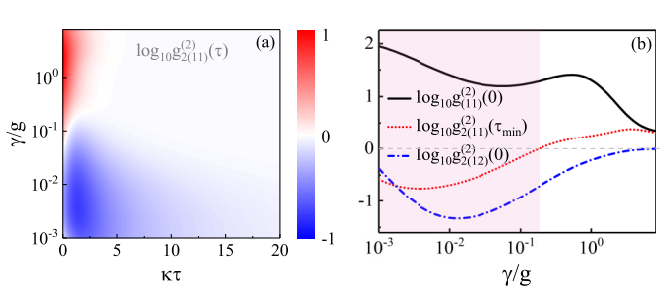

FIG. 8. (a) Logarithmic plot of the time-delayed second-order bundle correlation function $g^{(2)}_{2(11)}(\tau)$ as a function of the atom decay rate γ/g. (b) Logarithmic plot of the correlation functions $g^{(2)}_{(11)}(0)$, $g^{(2)}_{2(11)}(\tau_{\min})$, and $g^{(2)}_{2(12)}(0)$ for $\tau_{\min} = \sum_{m=1}^{N} 1/m\kappa$. The shadow area represents the regimes of $g^{(2)}_{2(11)}(\tau_{\min}) < 1$, $g^{(2)}_{2(12)}(0) < 1$, and $g^{(2)}_{(11)}(0) > 1$. The other parameters are the same as those in Fig. 3.

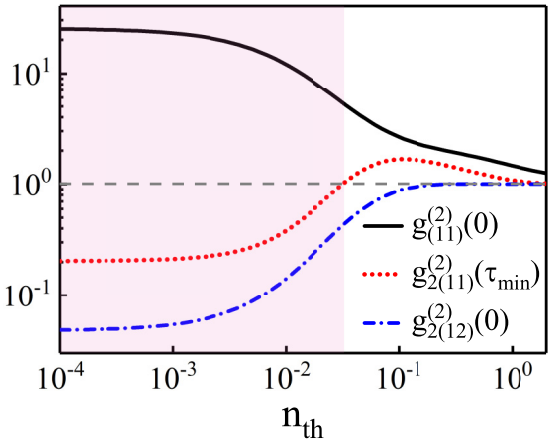

FIG. 9. The zero-time delayed correlation functions $g^{(2)}_{(11)}(0)$, $g^{(2)}_{2(11)}(\tau_{\min})$, and $g^{(2)}_{2(12)}(0)$ as a function of mean thermal photon numbers $n_{\rm th}$. The other parameters are the same as those in Fig. 3.

the master equation, Eq. (3), where $n_{{\rm th},l} = 1/(\exp(\frac{\hbar\omega_{a_l}}{K_B T}) - 1)$ are the equilibrium thermal photon occupation numbers with the Boltzmann constant K_B and the temperature T. Here we assume $n_{{\rm th},1} = n_{{\rm th},2} = n_{\rm th}$. In Fig. 9 the correlation functions $g^{(2)}_{(11)}(0)$, $g^{(2)}_{2(11)}(\tau_{\min})$, and $g^{(2)}_{2(12)}(0)$ are plotted as functions of the mean thermal photon number $n_{\rm th}$. It can be seen that the antibunched two-mode two-photon bundles, i.e., $g^{(2)}_{2(11)}(\tau_{\min}) < 1$, $g^{(2)}_{2(12)}(0) < 1$, and $g^{(2)}_{(11)}(0) > 1$, are achievable for $n_{\rm th} \leqslant 0.01$, which shows a strong robustness to the environmental noise.

V. EFFECT OF NONSYMMETRIC PARAMETERS

So far the bundle emission and the antibunching are analyzed for the symmetric parameters: $\omega_{a1} = \omega_{31}$ and $\omega_{a2} = \omega_{32}$ (i.e., $\delta_1 = \Delta_1$ and $\delta_2 = \Delta_2$), $\Delta_1 = -\Delta_2 = 24.5g$, $g_1 = g_2 = g$, $\gamma_1 = \gamma_2 = 0.01g$, and $\kappa_1 = \kappa_2 = 0.1g$. Such symmetry is possibly not so well realistic in practice. In this section we verify numerically the mechanism validity in a wide range of parameters. We plot in Fig. 10 the bundle correlation functions as functions of one parameter (Δ_1, g_1, γ_1, and κ_1, respectively) while the other parameters are fixed. It is obvious that all correlation functions are smaller than unity in a wide range of parameters. This means that the antibunching for the same modes and for the different modes is not so well sensitive to the parameter changes around the symmetric case. In particular, the cross-correlation function $g^{(2)}_{2(12)}(0)$ (blue dotted lines) remains almost unchanged in a wide range of the parameters. In comparison, the autocorrelation functions $g^{(2)}_{2(11)}(\tau_{\min})$ (red solid lines) and $g^{(2)}_{2(22)}(\tau_{\min})$ (green dashed lines) are a little more sensitive to the parameters. As shown in Fig. 10(a), the autocorrelation functions $g^{(2)}_{2(11)}(\tau_{\min})$ and $g^{(2)}_{2(22)}(\tau_{\min})$ take oscillating changes with the change in the detuning Δ_1. Nevertheless, the bundle antibunching in the same modes is well preserved in the range of $-1.3 < \Delta_1/\Delta_2 < -0.9$. Shown in Fig. 10(b), $g^{(2)}_{2(11)}(\tau_{\min})$ and $g^{(2)}_{2(22)}(\tau_{\min})$ increase as the coupling strength increases. Even so, good bundle antibunching in the same modes still stays in the range of $0 < g_1/g_2 < 1.5$. Figure10(c) shows a slight change of $g^{(2)}_{2(11)}(\tau_{\min})$ and

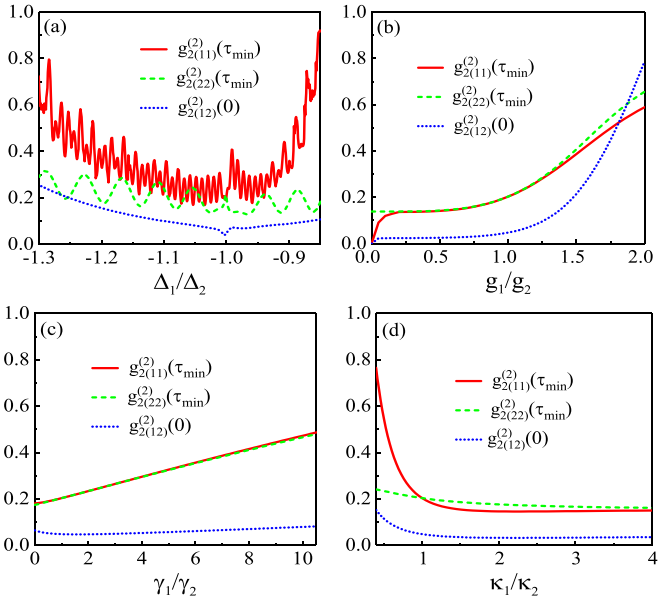

FIG. 10. The zero-time delayed correlation functions $g^{(2)}_{2(11)}(\tau_{\min})$, $g^{(2)}_{2(22)}(\tau_{\min})$, and $g^{(2)}_{2(12)}(0)$ as functions of (a) Δ_1, (b) g_1, (c) γ_1, and (d) κ_1. Except for the changing parameter, the fixed parameters are $\omega_{a1} = \omega_{31}$ and $\omega_{a2} = \omega_{32}$ (i.e., $\delta_1 = \Delta_1$ and $\delta_2 = \Delta_2$), $\Delta_1 = -\Delta_2 = 24.5g$, $g_1 = g_2 = g$, $\gamma_1 = \gamma_2 = 0.01g$, $\kappa_1 = \kappa_2 = 0.1g$, and $\Omega = 30g$.

$g^{(2)}_{2(22)}(\tau_{\min})$ with increasing γ_1. We find that the bundle antibunching in the same modes can be well realized even in the large range $0 < \gamma_1/\gamma_2 < 10$. Shown in Fig. 10(d) is the effect of the cavity dissipation κ_1. It can be seen that $g^{(2)}_{2(11)}(\tau_{\min})$ depends remarkably on κ_1 but is always smaller than unity when $\kappa_1/\kappa_2 \geqslant 0.4$. Meanwhile, the influence of the cavity decay rate κ_1 on $g^{(2)}_{2(22)}(\tau_{\min})$ is negligibly weak. Finally, when the changing parameters (Δ_1, g_1, γ_1, and κ_1) in Fig. 10 are substituted into (Δ_2, g_2, γ_2, and κ_2), respectively, the properties of autocorrelation functions $g^{(2)}_{2(11)}(\tau_{\min})$ and $g^{(2)}_{2(22)}(\tau_{\min})$ are exchanged, while the properties of the cross-correlation function $g^{(2)}_{2(12)}(\tau_{\min})$ remain unchanged. The two-photon bundle emission and the antibunching in the same and different modes are valid in a very wide range of parameters.

VI. CONCLUSION

We have shown that a Λ three-level system in a bimodal cavity can be used to continuously generate two-mode two-photon bundles. They arise from the leapfrog processes at different inner sidebands of the dressed atom, in which atomic coherence plays a key role. Two coherent channels can be selected by tuning the two cavity modes resonant with the bare atomic transitions, which ensures the antibunched two-photon bundles in the same modes and between different modes are obtained simultaneously. The antibunching for the different modes is based on the atomic coherence between the two final states of bundle emission, while the antibunching for the same modes is due to the dominance of cavity decay over atomic decay. These antibunched two-photon bundles have been shown to be robust against thermal photon noise and are achievable within a relatively wide range of parameters. Our work opens up a route to generate two-mode two-photon

states, which have potential applications in quantum information, high-precision metrology and ultrasensitive biosensing.

ACKNOWLEDGMENT

This work is supported by the National Natural Science Foundation of China (Grants No. 61875067 and No. 12274164).

APPENDIX: DERIVATION OF THE TWO-PHOTON SUPER-RABI OSCILLATION

In the dressed picture, the total Hamiltonian of the system is expressed as $H = H_0 + V$, where

$$H_0 = \delta_1 a_1^\dagger a_1 + \delta_2 a_2^\dagger a_2 + \bar{\Omega}(\sigma_{++} - \sigma_{--}), \tag{A1}$$

$$\begin{aligned} V =& g_1 a_1^\dagger \left[\sigma_{2L}^{(1)} + \sigma_L^{(1)} + \sigma_0^{(1)} + \sigma_R^{(1)} + \sigma_{2R}^{(1)}\right] \\ &+ g_2 a_2^\dagger \left[\sigma_{2L}^{(2)} + \sigma_L^{(2)} + \sigma_0^{(2)} + \sigma_R^{(2)} + \sigma_{2R}^{(2)}\right] + \text{H.c.} \end{aligned} \tag{A2}$$

Then an effective Hamiltonian can be obtained by applying the unitary transformation $H_{\text{eff}} = \exp(-\lambda S) H \exp(\lambda S)$, where we introduce the non-Hermitian operator

$$\begin{aligned} S =& g_1 a_1 \left[\frac{1}{\delta_1 - 2\bar{\Omega}}\sigma_{2L}^{(1)} + \frac{1}{\delta_1 - \bar{\Omega}}\sigma_L^{(1)} + \frac{1}{\delta_1}\sigma_0^{(1)} \right. \\ &\left. + \frac{1}{\delta_1 + \bar{\Omega}}\sigma_R^{(1)} + \frac{1}{\delta_1 + 2\bar{\Omega}}\sigma_{2R}^{(1)}\right] \\ &+ g_2 a_2 \left[\frac{1}{\delta_2 - 2\bar{\Omega}}\sigma_{2L}^{(2)} + \frac{1}{\delta_2 - \bar{\Omega}}\sigma_L^{(2)} + \frac{1}{\delta_2}\sigma_0^{(2)} \right. \\ &\left. + \frac{1}{\delta_2 + \bar{\Omega}}\sigma_R^{(2)} + \frac{1}{\delta_2 + 2\bar{\Omega}}\sigma_{2R}^{(2)}\right] - \text{H.c.}, \end{aligned} \tag{A3}$$

with the satisfaction of $V + [H_0, S] = 0$. The parameter λ is introduced to represent the degree of perturbation and we rewrite V as λV. In terms of the Baker-Campbell-Hausdorff formula, we expand H_{eff} to second-order in λ:

$$\begin{aligned} H_{\text{eff}} =& H_0 + \lambda V - \lambda[S, H_0] - \lambda^2[S, V] \\ &+ \frac{\lambda^2}{2!}[S, [S, H_0]] + O(\lambda^3) \\ =& H_0 - \frac{\lambda^2}{2}[S, V] + O(\lambda^3). \end{aligned} \tag{A4}$$

By setting $\lambda = 1$ and driving the system to the two-photon resonance $\delta = \bar{\Omega}/2$, the related second-order perturbation interaction Hamiltonian is reduced to three terms, $H_{\text{eff}}^{(2)} = H_{\text{eff},1}^{(2)} + H_{\text{eff},2}^{(2)} + H_{\text{eff},12}^{(2)}$, with

$$H_{\text{eff},1}^{(2)} = -\frac{g_1^2}{2} a_1^2 (G_1 \sigma_{0-} + G_2 \sigma_{+0}) + \text{H.c.}, \tag{A5}$$

$$H_{\text{eff},2}^{(2)} = -\frac{g_2^2}{2} a_2^2 (G_1 \sigma_{0+} + G_2 \sigma_{-0}) + \text{H.c.}, \tag{A6}$$

$$H_{\text{eff},12}^{(2)} = -\frac{g_1 g_2}{2} G_3 a_1 a_2 (\sigma_{++} - \sigma_{--}) + \text{H.c.} \tag{A7}$$

The first and second terms represent the two-photon transitions for cavity modes a_1 and a_2, respectively. The second term denotes the two-photon transition composed of an a_1 photon and an a_2 photon. The coupling coefficients are defined as

$$G_1 = \frac{4}{\bar{\Omega}} A_+ (C_+ + D) + \frac{4}{3\bar{\Omega}} A_- C_+, \tag{A8}$$

$$G_2 = \frac{4}{\bar{\Omega}} B (C_- - D) + \frac{4}{3\bar{\Omega}} B C_+, \tag{A9}$$

$$G_3 = \frac{4}{15\bar{\Omega}} [3C_-^2 + 5(C_+^2 + A_- B) - 15 A_+ B]. \tag{A10}$$

Similarly, when $\delta = -\bar{\Omega}/2$, the corresponding Hamiltonian is divided as follows: $\tilde{H}_{\text{eff}}^{(2)} = \tilde{H}_{\text{eff},1}^{(2)} + \tilde{H}_{\text{eff},2}^{(2)} + \tilde{H}_{\text{eff},12}^{(2)}$, with

$$\tilde{H}_{\text{eff},1}^{(2)} = -\frac{g_1^2}{2} a_1^2 (\tilde{G}_1 \sigma_{0+} + \tilde{G}_2 \sigma_{-0}) + \text{H.c.}, \tag{A11}$$

$$\tilde{H}_{\text{eff},2}^{(2)} = -\frac{g_2^2}{2} a_2^2 (\tilde{G}_1 \sigma_{0-} + \tilde{G}_2 \sigma_{+0}) + \text{H.c.}, \tag{A12}$$

$$\tilde{H}_{\text{eff},12}^{(2)} = -\frac{g_1 g_2}{2} \tilde{G}_3 a_1 a_2 (\sigma_{++} - \sigma_{--}) + \text{H.c.}, \tag{A13}$$

where the coupling coefficients are defined as

$$\tilde{G}_1 = -\frac{4}{\bar{\Omega}} A_- (D - C_-) + \frac{4}{3\bar{\Omega}} A_+ C_-, \tag{A14}$$

$$\tilde{G}_2 = -\frac{4}{\bar{\Omega}} B (C_+ + D) - \frac{4}{3\bar{\Omega}} B C_-, \tag{A15}$$

$$\tilde{G}_3 = \frac{4}{15\bar{\Omega}} [3C_+^2 + 5(C_-^2 - A_+ B) + 15 A_- B]. \tag{A16}$$

[1] J. L. O'Brien, A. Furusawa, and J. Vučković, Photonic quantum technologies, Nat. Photonics **3**, 687 (2009).

[2] C. H. Bennett and D. P. DiVincenzo, Quantum information and computation, Nature (London) **404**, 247 (2000).

[3] E. Knill, R. Laflamme, and G. J. Milburn, A scheme for efficient quantum computation with linear optics, Nature (London) **409**, 46 (2001).

[4] L.-M. Duan and H. J. Kimble, Scalable Photonic Quantum Computation through Cavity-Assisted Interactions, Phys. Rev. Lett. **92**, 127902 (2004).

[5] L.-M. Duan, M. D. Lukin, J. I. Cirac, and P. Zoller, Long-distance quantum communication with atomic ensembles and linear optics, Nature (London) **414**, 413 (2001).

[6] V. Scarani, H. Bechmann-Pasquinucci, N. J. Cerf, M. Dušek, N. Lütkenhaus, and M. Peev, The security of practical quantum key distribution, Rev. Mod. Phys. **81**, 1301 (2009).

[7] I. Afek, O. Ambar, and Y. Silberberg, High-NOON states by mixing quantum and classical light, Science **328**, 879 (2010).

[8] H. J. Kimble, The quantum internet, Nature (London) **453**, 1023 (2008).

[9] V. Giovannetti, S. Lloyd, and L. Maccone, Quantum Metrology, Phys. Rev. Lett. **96**, 010401 (2006).

[10] M. D'Angelo, M. V. Chekhova, and Y. Shih, Two-Photon Diffraction and Quantum Lithography, Phys. Rev. Lett. **87**, 013602 (2001).

[11] J. C. López Carreño, C. Sánchez Muñoz, D. Sanvitto, E. del Valle, and F. P. Laussy, Exciting Polaritons with Quantum Light, Phys. Rev. Lett. **115**, 196402 (2015).

[12] K. E. Dorfman, F. Schlawin, and S. Mukamel, Nonlinear optical signals and spectroscopy with quantum light, Rev. Mod. Phys. **88**, 045008 (2016).

[13] W. Denk, J. H. Strickler, and W. W. Webb, Two-photon laser scanning fluorescence microscopy, Science **248**, 73 (1990).

[14] N. G. Horton, K. Wang, D. Kobat, C. G. Clark, F. W. Wise, C. B. Schaffer, and C. Xu, In *vivo* three-photon microscopy of subcortical structures of an intact mouse brain, Nat. Photonics **7**, 205 (2013).

[15] C. S. Muñoz, E. del Valle, A. G. Tudela, K. Müller, S. Lichtmannecker, M. Kaniber, C. Tejedor, J. J. Finley, and F. P. Laussy, Emitters of N-photon bundles, Nat. Photonics **8**, 550 (2014).

[16] C. Sánchez Muñoz, F. P. Laussy, C. Tejedor, and E. del Valle, Enhanced two-photon emission from a dressed biexciton, New J. Phys. **17**, 123021 (2015).

[17] Y. Chang, A. González-Tudela, C. S. Muñoz, C. Navarrete-Benlloch, and T. Shi, Deterministic Down-Converter and Continuous Photon-Pair Source within the Bad-Cavity Limit, Phys. Rev. Lett. **117**, 203602 (2016).

[18] C. Sánchez Muñoz, F. P. Laussy, E. del Valle, C. Tejedor, and A. González-Tudela, Filtering multiphoton emission from state-of-the-art cavity quantum electrodynamics, Optica **5**, 14 (2018).

[19] Q. Bin, X.-Y. Lü, F. P. Laussy, F. Nori, and Y. Wu, N-Phonon Bundle Emission via the Stokes Process, Phys. Rev. Lett. **124**, 053601 (2020).

[20] Q. Bin, Y. Wu, and X.-Y. Lü, Parity-Symmetry-Protected Multiphoton Bundle Emission, Phys. Rev. Lett. **127**, 073602 (2021).

[21] M. Cosacchi, A. Mielnik-Pyszczorski, T. Seidelmann, M. Cygorek, A. Vagov, D. E. Reiter, and V. M. Axt, N-photon bundle statistics in different solid-state platforms, Phys. Rev. B **106**, 115304 (2022).

[22] S.-L. Ma, X.-K. Li, Y.-L. Ren, J.-K. Xie, and F.-L. Li, Antibunched N-photon bundles emitted by a Josephson photonic device, Phys. Rev. Res. **3**, 043020 (2021).

[23] S.-L. Ma, J.-K. Xie, Y.-L. Ren, X.-K. Li, and F.-L. Li, Photon-pair blockade in a Josephson-photonics circuit with two nondegenerate microwave resonators, New J. Phys. **24**, 053001 (2022).

[24] Y. Deng, T. Shi, and S. Yi, Motional n-phonon bundle states of a trapped atom with clock transitions, Photonics Res. **9**, 1289 (2021).

[25] F. Zou, J.-Q. Liao, and Y. Li, Dynamical emission of phonon pairs in optomechanical systems, Phys. Rev. A **105**, 053507 (2022).

[26] S.-Y. Jiang, F. Zou, Y. Wang, J.-F. Huang, X.-W. Xu, and J.-Q. Liao, Multiple-photon bundle emission in the n-photon Jaynes-Cummings model, arXiv:2204.09899.

[27] T. Jennewein, C. Simon, G. Weihs, H. Weinfurter, and A. Zeilinger, Quantum Cryptography with Entangled Photons, Phys. Rev. Lett. **84**, 4729 (2000).

[28] D. S. Naik, C. G. Peterson, A. G. White, A. J. Berglund, and P. G. Kwiat, Entangled State Quantum Cryptography: Eavesdropping on the Ekert Protocol, Phys. Rev. Lett. **84**, 4733 (2000).

[29] D. Bouwmeester, J.-W. Pan, K. Mattle, M. Eibl, H. Weinfurter, and A. Zeilinger, Experimental quantum teleportation, Nature (London) **390**, 575 (1997).

[30] I. Marcikic, H. de Riedmatten, W. Tittel, H. Zbinden, and N. Gisin, Long-distance teleportation of qubits at telecommunication wavelengths, Nature (London) **421**, 509 (2003).

[31] J.-W. Pan, D. Bouwmeester, H. Weinfurter, and A. Zeilinger, Experimental Entanglement Awapping: Entangling Photons That Never Interacted, Phys. Rev. Lett. **80**, 3891 (1998).

[32] F. Troiani, Entanglement swapping with energy-polarization-entangled photons from quantum dot cascade decay, Phys. Rev. B **90**, 245419 (2014).

[33] C. Simon, H. de Riedmatten, M. Afzelius, N. Sangouard, H. Zbinden, and N. Gisin, Quantum Repeaters with Photon Pair Sources and Multimode Memories, Phys. Rev. Lett. **98**, 190503 (2007).

[34] B. Bell, S. Kannan, A. McMillan, A. S. Clark, W. J. Wadsworth, and J. G. Rarity, Multicolor Quantum Metrology with Entangled Photons, Phys. Rev. Lett. **111**, 093603 (2013).

[35] P. Lesani, G. Singh, C. M. Viray, Y. Ramaswamy, D. M. Zhu, P. Kingshott, Z. F. Lu, and H. Zreiqat, Two-photon dual-emissive carbon dot-based probe: deep-tissue imaging and ultrasensitive sensing of intracellular ferric ions, ACS Appl. Mater. Interfaces **12**, 18395 (2020).

[36] M. O. Scully and M. S. Zubairy, *Quantum Optics* (Cambridge University, Cambridge, England, 1997).

[37] D. F. Walls and G. J. Milburn, *Quantum Optics* (Springer-Verlag, Berlin, 1994).

[38] J. R. Johansson, P. D. Nation, and F. Nori, QuTiP: An open-source Python framework for the dynamics of open quantum systems, Comput. Phys. Commun. **183**, 1760 (2012).

[39] C. Cohen-Tannoudji, J. Dupont-Roc, and G. Grynberg, *Atom-Photon Interactions* (Wiley, New York, 1992).

[40] J. C. López Carreño, E. del Valle, and F. P. Laussy, Photon correlations from the Mollow triplet, Laser Photonics Rev. **11**, 1700090 (2017).

[41] B. R. Mollow, Power spectrum of light scattered by two-level systems, Phys. Rev. **188**, 1969 (1969).

[42] R. J. Glauber, The quantum theory of optical coherence, Phys. Rev. **130**, 2529 (1963).

[43] F. Boitier, A. Godard, E. Rosencher, and C. Fabre, Measuring photon bunching at ultrashort timescale by two-photon absorption in semiconductors, Nat. Phys. **5**, 267 (2009).